A new strategy for upgrading ventilation air methane emissions combining adsorption and combustion in a lean-gas turbine

*David Ursueguía, Pablo Marín, Eva Díaz and Salvador Ordóñez**

Catalysis, Reactors and Control Research Group (CRC)

Department of Chemical and Environmental Engineering

University of Oviedo, 33006, Spain

*Correspondence: sordonez@uniovi.es

ABSTRACT

This work evaluates the feasibility of harnessing a high-flow (4.4 Nm^3/s) and low-concentrated (0.57% CH_4) methane stream from a coal mine ventilation emission. Two consecutive processes have been coupled: a fixed bed adsorption used for methane concentration by temperature-swing adsorption, and a combustion process in a lean-gas turbine. Both processes have been simulated using rigorous mathematical model implemented in a commercial simulation package. Regarding the adsorption concentration step, optimized results showed the possibility of obtaining an outlet stream with 1.2% CH_4 and a total flowrate of 3.8 Nm^3/s. The gas turbine generates a net energy output of 490 kW and provides the heating required in the desorption step. The process design has been completed with an economic evaluation of the process. The estimated initial investment of the process is high (4.74 M€), and the return profitability depends a lot on the cost of the adsorbent material. The process would be profitable in a 20-year period with a 4.25% discount rate for an adsorbent cost lower than 0.6 €/kg.

Keywords: Ventilation air methane; Lean-fuel turbine; Temperature-swing adsorption; Process integration; Process simulation

1. INTRODUCTION

The concern about the role of methane emissions in the anthropogenic global warming effect has been increased in the last years [1-3]. These emissions are not only a source of environmental concern, but also represent a large amount of wasted energy. Among these emissions, coal mines emissions are of key importance, even in the case of abandoned coal mines. The huge increase in these emissions and its climatic consequences have generated a significant global awareness, and strengthened the need of alternative or less harmful procedures to obtain energy and chemicals. Following this trend, the option of capturing and upgrading these emissions has emerged in recent times [4, 5]. In fact, this capture and harnessing would entail two advantages: the greenhouse emissions reduction and the use of a resource that otherwise would be wasted.

There are mainly three different types of mining emissions containing methane: coal bed methane (CBM), abandoned mine methane (AMM) and ventilation air methane (VAM). The first two contain high and medium purity methane (> 30%) and are easily usable with well-known harnessing technologies available. The VAM has a very low concentration (0.1-1%), so it is usually burned with very low energy efficiency [6-8] or even directly released to the atmosphere [9, 10]. Low concentration methane streams are typically generated in areas where workers and facilities need protection from asphyxiations and explosions. The objective is to keep work areas out of the explosive methane/air limit [11]. Extraction systems in coal mines are mainly fans properly situated in order to ensure adequate and safe conditions, even after the shaft is abandoned [9]. The large flows emitted and the poor development in harnessing techniques made VAM emissions to account for up to 90% of all methane emissions from coal mining [12]. Therefore, the challenge is to upgrade these low purity streams and transform them into a more sustainable energy source or raw material.

The research addressed in the present work has been performed in the context of the European Research Project METHENERGY+, focused on VAM mitigation and upgrading. Different European coal basins were considered: Upper Silesian Basin (Poland and Czech Republic), Asturian Basin (Spain) and Velenje Basin (Slovenia). These mines present VAM average concentrations in the range 0.1 to 0.3% CH_4 with very high total flowrates (even as high as 200 Nm^3/s). The characteristics of VAM (i.e. flowrate and methane concentration) depend on the mining exploitation and varies upon time. In fact, measurements reported by other authors for mining exploitations from other parts of the world show the possibility of higher VAM concentration, up to 0.9% or even higher [13-15]. These differences may be due to the type of coal extracted, the configuration of the shafts, the safety regulations or the

efficiency of the ventilation processes; some of these exploitations have low ventilation flow rates (less than 1 m^3/s). Therefore, based on average results of several authors, a stream with fair to moderate methane concentration and air flowrate values has been selected for the analysis made in the present work: 0.57% CH_4 and 4.4 Nm^3/s, respectively.

The recovery of the energy associated to methane from coal mine ventilation air emissions can be done using lean-burn gas turbines (EDL, CSIRO, IR, etc.). These type of turbines are especially suited to work with low methane concentrations and are able to produce work (electricity) directly. Lean-burn turbines are not widely used for the harnessing of VAM, because they require a minimum methane concentration of 1% [16], which is rather high for most VAM emissions. Hence, a previous methane concentration step is needed. Still, there are some cases, such as, the cost-effective lean-burn turbine designed by Su et al. [17], which have obtained 19-21 kWe of electricity output with an inlet stream with 0.8% CH_4 in air.

Methane concentration can be achieved by fixed bed adsorption. This is one of the major promising technologies for methane concentration, providing good yields and adequate concentrations for the operation of the gas turbine [18, 19]. Temperature-swing adsorption (TSA) is the most economically feasible, given the lower energy requirements [20], and also the adsorption technique recommended for concentrations lower than 2% [21, 22].

One of the key parameters in TSA processes is the proper selection of the adsorbent material. In this work, we consider two types of adsorbents: metal-organic frameworks (MOFs) and activated carbons. The first have been widely studied and stand out above the others, especially in pure methane gravimetric capacity comparison [23, 24]. MOFs are known for its exceptional storage capacity for gases, such as, hydrogen, methane and carbon dioxide [25]. Active carbons have lower adsorption capacity and selectivity. However, they are major competitors because of their lower cost [26]. Another important parameter is the desorption temperature, related to the energy required to recover the methane concentrated stream from the adsorbent. Studies done by other authors indicate that methane adsorption enthalpy is not very high, which means that the desorption temperature is low [27, 28]. Additionally, the energy required for the desorption step could be obtained from the effluent of the gas turbine [29].

The objective of the present work is the harnessing of a VAM stream using an adsorption/desorption unit, as a first pre-concentration step, and a lean-burn gas turbine to produce electricity. First, the adsorbent material has been selected and the fixed-bed adsorption unit designed. Then, the desorption step has been simulated using Aspen

Adsorption software, in order to predict the concentration of methane in the stream sent to the gas turbine. The performance of the lean-burn gas turbine has been simulated using Aspen Hysys and the optimum operating conditions have been determined. The integration of the adsorption/desorption unit with the gas turbine has been evaluated for improving the economy of the overall processes. Finally, the economic evaluation of the process has been presented.

2. METHODOLOGY

2.1. Flowsheet of integrated harnessing process

The harnessing of coal mine ventilation air methane (VAM) emissions has been proposed according to a two-step integrated process: methane concentration in an adsorption/desorption unit, followed by methane combustion in a lean-burn gas turbine. The flowsheet of this process is depicted in Fig. 1.

The concentration step is carried out in a fixed bed temperature-swing adsorption (TSA) operation. This unit is inherently discontinuous, with adsorption happening in a first step and, once the adsorbent is saturated, methane in recovered by desorption at a higher temperature. The concentration step must increase methane concentration to a minimum of 1%, in order to use a lean-burn gas turbine for the combustion.

The lean-burn gas turbine is made of three elements: compressor, recuperator and turbine. The turbine is able of generating net work and, hence, produce electricity. The recuperator is used to pre-heat the feed before the combustion using the part of the energy of the combustion gases. In addition, part of these combustion gases can be used as the drag stream of the desorption process [30], as shown in Fig. 1. This level of mass and heat integration is critical, in order to save energy and improve the economy of the process.

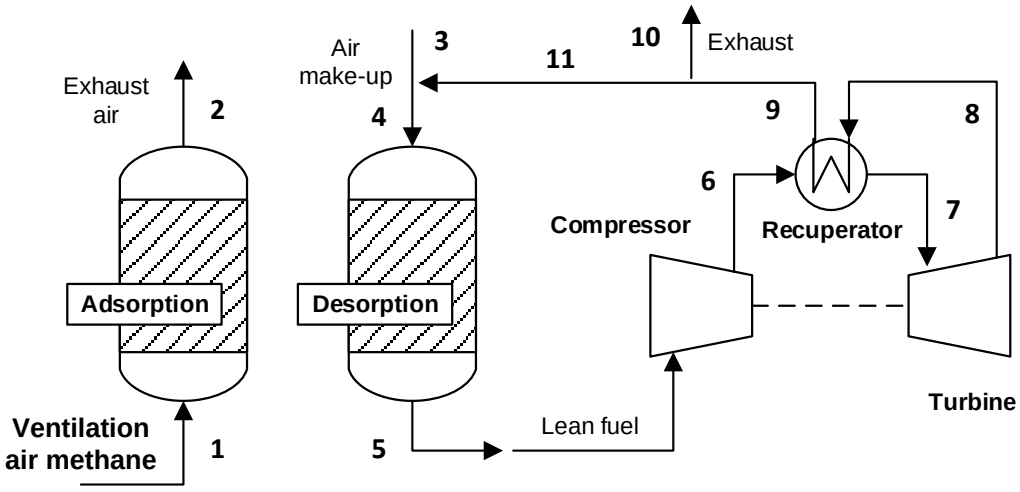

Figure 1. Flowsheet of the TSA-turbine integrated process.

2.2. Selection of the adsorbent material

Both metal organic frameworks (MOF) and active carbons have properties that make them feasible adsorbents for methane. The outstanding properties of MOFs are conferred by large specific surface areas, high pore volume, great porosity and the massive presence of metallic adsorption sites. Regarding active carbons, its low cost, high porosity and large specific surface area stand out as properties. The bottleneck of the process is the separation of methane from nitrogen, as both molecules are very similar in size (3.82 and 3.64 Å, respectively), both have zero dipole and a little higher polarizability in the case of methane ($26 \cdot 10^{-25}$ and $17.6 \cdot 10^{-25}$ cm^3, respectively).

Active carbons are commonly used for the separation of volatile organic compounds, where the molecular size of the organic molecules and nitrogen or oxygen is quite different [31]. However, the reported adsorption capacity for methane/nitrogen mixtures is low, e.g., for a commercial activated carbon Norit RB3 methane saturation is 6.75 mmol/g and methane/nitrogen selectivity 1.3 [32]. Its low adsorption capacity questions the possibility of reaching product streams with concentrations high enough to operate the subsequent turbine. On the other hand, separation capacity of MOFs is higher [33]. In many cases, the enhance adsorption capacity is caused by the presence of active metallic sites in the structure, since differences in polarity or polarizability of adsorbate molecules can mean also differences in attraction by these metallic centres through electrostatic interactions [34]. Among the MOFs, Basolite C300 has exceptional yields in gas separation processes [35], in addition to be one of the best performing materials for methane adsorption and storage [36]. Laboratory research on this material has shown the ability to separate methane and nitrogen mixtures at low pressures, obtaining pure methane/nitrogen selectivity up to 2.2 at 0.1 MPa and 298 K [37]. Therefore, Basolite C300 is selected as adsorbent material for the design of the adsorption/desorption unit.

From adsorption isotherms obtained for methane/nitrogen mixtures at 298 K, and also considering the maximum adsorption capacities for both pure gases at different temperatures on Basolite C300 [37], methane/nitrogen adsorption isotherms can be approximated from the initial isotherm at different temperatures (293-353 K). In the approximation, it is supposed that the relative variations in total adsorption gravimetric capacity for each gas ($P_P = 1$) is practically the same in all the points that conform the isotherm ($P_P < 1$). This approximation can be done

at low pressures, in which the isotherm shape is similar for all temperatures [38]. Further, similarity in behaviour of nitrogen and oxygen isotherms on Basolite C300 [39], as well as, the large presence of nitrogen in the streams to be treated allow performing the simulation using methane/nitrogen isotherms, with low deviation and even being a conservative design, since nitrogen adsorption capacity is higher than for oxygen. Isotherms obtained are fit to a simple Langmuir model (Eq. 1), and the fitting parameters are presented in Table 1.

$$q_e = \frac{q_m K_L P_P}{1 + K_L P_P} \;\; ; \; K_L = \; K_{L0} e^{\frac{-\Delta H}{RT}} \qquad \text{(Eq. 1)}$$

Values of q_m are independent of temperature, whereas K_L depends strongly on it [40]. Temperature dependence of K_L can be approximated by Van't Hoff equation (Eq. 5). This model predicts the equilibrium values of both gases at each partial pressure and temperature. For example, at 298 K and 0.1% CH_4 at 100 kPa, methane adsorption capacity is 0.095 mg/g and nitrogen adsorption capacity is 35.68 mg/g.

Table 1. Langmuir model parameters for methane/nitrogen adsorption [37].

Component	*Methane*	*Nitrogen*
q_m (mg g^{-1})	81.96	77.51
K_{L0} (kPa^{-1})	$7.45 \cdot 10^{-8}$	$4.30 \cdot 10^{-8}$
ΔH (kJ mol^{-1})	-29.5	-30.2

2.3. *Adsorption/desorption simulation*

Prior to real scale experimentation, given the investment costs involved, it is proposed the modelling and simulation of a large scale operation that fits as close as possible to the real process. The generation of a realistic model in an appropriate simulation software allows obtaining results for different initial values, making comparisons in key parameters and deciding the best conditions to carry it out, which could be based on economic or yield criteria. Adsorption is fixed bed can be modelled, and the breakthrough curves predicted, using a dynamic heterogeneous one-dimensional model. The following assumptions have been considered to develop the model equations: isothermal conditions, negligible radial gradients (of fluid velocity, bed void, dispersion coefficient, etc.) and spherical homogeneous adsorbent particle. The gas phase mass balance (Eq. 2) includes, respectively, accumulation, convection flow, axial dispersion, and interphase mass transfer terms. The solid phase mass balance (Eq. 3) is formed by accumulation and interphase mass transfer terms.

$$\frac{\partial C_i}{\partial t} = -\frac{u_0}{\varepsilon_b}\frac{\partial C_i}{\partial Z} + D_e\frac{\partial^2 C_i}{\partial Z^2} - 15\frac{4\rho_b(1-\varepsilon_b)}{\varepsilon_b {d_p}^2} D_i\left(W_{ieq} - W_i\right) \quad \text{(Eq. 2)}$$

$$\frac{\partial W_i}{\partial t} = 15\frac{4}{{d_p}^2} D_i\left(W_{ieq} - W_i\right) \quad \text{(Eq. 3)}$$

Interphase mass transfer has been modelled using a linear driving force (LDF) expression. This model relates mass transport and the adsorption equilibrium, calculated using the Langmuir adsorption isotherms (Eq. 1). This relation depends on the mass-transfer resistances for the transport of the adsorbate from the bulk gas phase to the adsorbent surface. In case of an adsorbent made of micropores, like MOFs, the adsorption mass transfer rate is controlled by diffusion in the micropore network (as indicated in Eq. 2 and 3).

This model has been validated in the scope of a previous work using break curves obtained in a Basolite C300 fixed-bed and working for different methane/nitrogen concentrations [41].

Desorption of methane is carried out using a drag gas and an increase of temperature, i.e., temperature-swing adsorption (TSA). Hence, the model must be completed with the incorporation of the energy balance to the gas and solid phases (Eq. 4 and 5):

$$\frac{\partial T_g}{\partial t} = -u_0\frac{\partial T_g}{\partial Z} + h_s\frac{a_p}{C_{pg}\rho_g}\left(T_s - T_g\right) \quad \text{(Eq. 4)}$$

$$\frac{\partial T_s}{\partial t} = h_s\frac{a_p}{C_{ps}\rho_b}\left(T_g - T_s\right) \quad \text{(Eq. 5)}$$

In the heating stage, the drag gas enters the fixed bed at elevated temperature, so there is an initial thermal gradient between solid and gas phases [42]. The velocity at which thermal equilibrium is reached depends on the heat transfer coefficient (h_s), calculated using correlations for fixed-beds based on Nusselt and Prandtl dimensionless numbers [43]. Additional parameters, such as, the specific heat capacity (C_{ps}) are obtained from other works [44]. Variations in temperature through the bed and upon time affect the equilibrium adsorption, predicted using Eq. 1. On the other hand, the cooling stage is similar but with air passing at the adsorption temperature.

This set of differential equations, combined with the adsorbent and inlet flow properties, as well as with the adsorption isotherm equation, are able of predicting the behaviour of VAM adsorption. It is possible to obtain the breakthrough adsorption curve, the concentration of the adsorbates in the solid at saturation conditions, the corresponding desorption curve and the outlet methane concentration obtained at the end of the concentration stage.

The previous model equations have been solved with the help of Aspen Adsorption software. Fig. 2 shows the corresponding flowsheet diagram. The discretization method used to solve

the equations is UDS1 with 20 nodes. Momentum balance is calculated through Ergun equation.

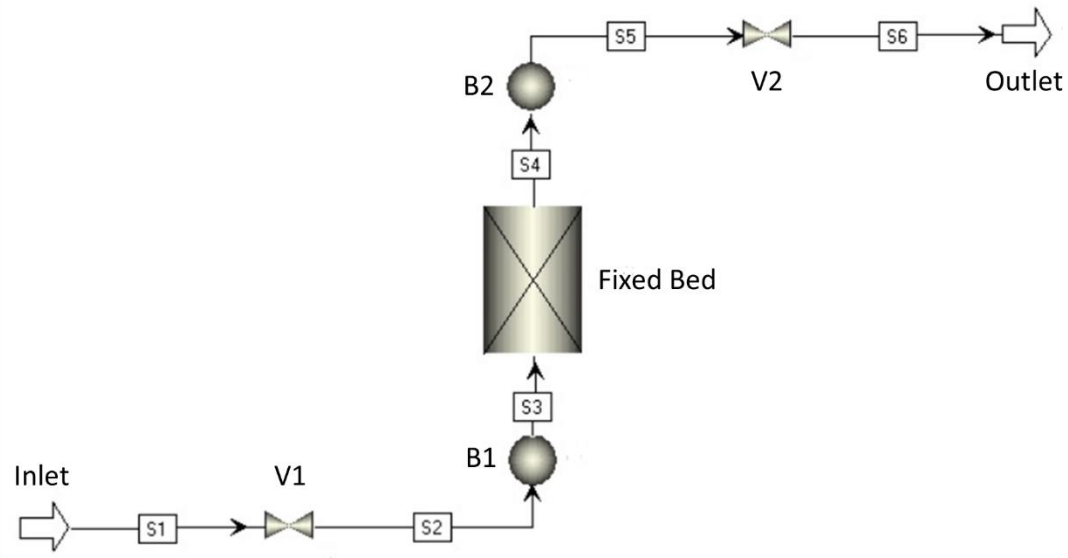

Figure 2. Aspen Adsorption flowsheet diagram for a single-bed adsorption/desorption process.

2.4. Lean-burn turbine simulation

The lean-burn turbine has been simulated using Aspen Hysys. The flowsheet diagram of the process, shown in Fig. 3, is formed by three elements [17]: a compressor, a heat exchanger or recuperator, a conversion reactor and an expander.

The compressor is used to increase the pressure of the gas feed (100 kPa); the main design parameter being the pressure ratio (outlet pressure/feed pressure). The compressor is modelled as a single-stage centrifugal compressor with adiabatic efficiency of 75%. In the compressor, temperature also increases, but, in lean-burn turbines, this increase is not enough to trigger the combustion, because methane concentration is below the lower flammability limit (< 5%). Hence, temperature must be increased, at least to 1073 K, using a heat exchanger, called recuperator. The area required by the recuperator is calculated assuming a global heat transfer coefficient of 0.01 kW/m^2 K (typical of gas-to-gas heat exchangers).

The methane combustion reaction has been modelled using a conversion reactor with 100% methane conversion. The combustion gases are expanded to recover part of their energy as work. An expander with an isentropic efficiency of 75% is used in the model. Finally, the exhaust of the expander, which is at high temperature, is used to supply the energy required in the recuperator.

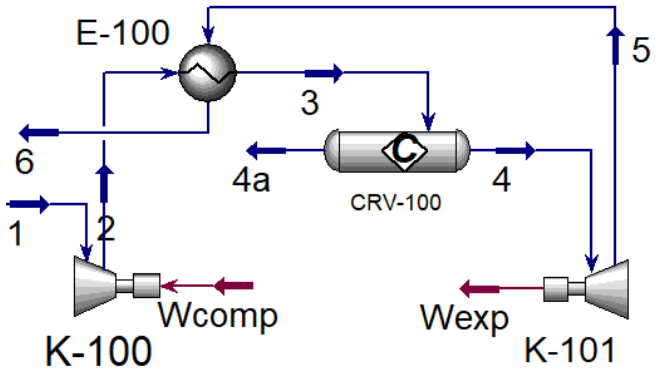

Figure 3. Flowsheet diagram for the simulation of a lean-burn turbine in Aspen Hysys.

3. RESULTS AND DISCUSSION

3.1. Design of fixed bed adsorption/desorption unit

Fixed beds are generally vertical columns with set dimensions and filled with a fixed amount of adsorbent, necessary to reach the performance specifications in both adsorption and desorption processes, which usually are consecutive. The length and diameter depend on the inlet flowrate, as well as on the volume required for locating the required solid adsorbent loading. Likewise, the choice of the adsorbent particle size is also for preventing large pressure drops and ensuring good gas-solid contact. As Gabelman [45] has indicated, surface velocity and particle size selection, and diameter and bed length calculation are the four basic points to estimate in order to make a successful fixed bed design. These parameters, in addition to the operation temperature, could change the final yield of the operation. Table 2 shows the general effects of these parameters on the final adsorption and desorption performance.

The surface velocity provides enough residence time for the required adsorption, and an acceptable pressure drop. Typical surface velocities for gases in a fixed bed are between 0.2 and 0.5 m/s [46]. In case of Basolite C300, 0.24 m/s is selected as surface velocity for adsorption, whereas 0.48 m/s for desorption. Continuing with particle size (d_p), in general, the smallest the particle size, the highest the mass-transfer rate, due to the shorter particle diffusion path. Overall, selected particle sizes are generally those that allow the best contact with allowable pressure drops, so a compromise is necessary.

Table 2. Effect of an increase of several operational parameters on the adsorption and desorption performance.

Parameter	Typical range	Affects to*
Bed length	0-14 m	Fixed bed efficiency (+), breakthrough time (+), pressure drop (+), total costs (+) and cycle time (+)
Bed diameter	0-3.5 m	Surface velocity (-), isothermal fixed bed thermal regime (-) and number of total neccesary parallel fixed beds (-)
Surface velocity	0.2-0.5 m/s	Residence time (-), breakthrough time (-), pressure drop (+), product dilution (-) and cycle time (-)
Particle diameter	0.5-10 mm	Solid-gas contact (-) and pressure drop (-)
Temperature	Upper limit: material decomposition	Adsorption capacity (-), total costs (+) and desorption capacity (+)

* (+) means an increase and (-) a decrease respect to the increase in the studied parameter.

Pressure drop can be estimated by a mechanical balance (Ergun equation, Eq. 6). Gas physical properties as viscosity (μ_g = $1.7 \cdot 10^{-5}$ Pa·s) and density (ρ_g = 1.18 kg/m^3) are known at adsorption temperature (298 K), as well as, surface velocity (u_0 = 0.24 m/s) and bed porosity (ε_b), which is supposed to be close to 0.4, considering particles almost spherical and randomly packed [47]. Typical particle sizes in an industrial operation are between 0.5 and 10 mm [46]. Based on Fig. 4, particles from 2 mm onwards could be used, even in fairly long beds, for both adsorption and desorption processes. Temperature selected in the desorption process is 343 K.

$$\frac{\partial P}{\partial Z} = \frac{150\mu_g(1-\varepsilon_b)^2}{d_p^2\varepsilon_b^3}u_0 + \frac{1.75\rho_g(1-\varepsilon_b)}{d_p\varepsilon_b^3}u_0^2 \qquad \text{(Eq. 6)}$$

Once the surface velocity, the particle size and the characteristics of the input stream are known, it is possible to calculate the appropriate dimensions of the fixed bed [48]. Couper et al. [46] have indicated that the range of typical operating time for a gas phase in an adsorption process is between 0.5 and 8 hours. Adsorbers 14 m high and 3.5 m in diameter, as maximum

sizes, are typically in use. In fact, bed utilization efficiency increases with bed length, because the part of unused bed becomes a smaller portion [45], but also increases the operative fixed costs and the total pressure drop.

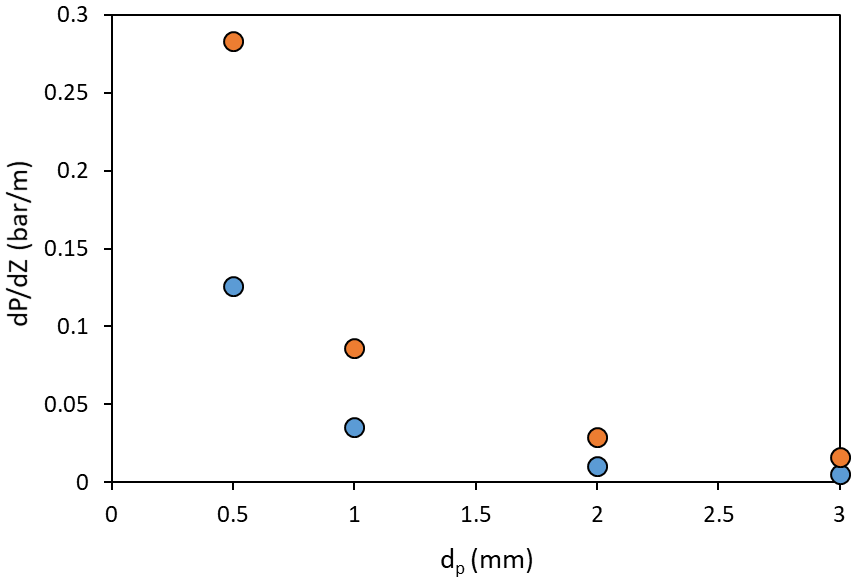

Figure 4. Pressure drop, calculated by Ergun equation (Eq. 6), in function of total fixed bed length (bar/m) in the process, for different adsorbent particle sizes. Adsorption (blue circles) and desorption (orange circles).

Diameter selection should also take into account the exothermic nature of adsorption, in order to avoid great temperature increments during the process, thus a relative high surface-to-volume ratio is desirable [48]. In this case, the total inlet flow rate is high (4.4 Nm^3/s), so 4 equal fixed beds are assumed to be working in parallel at the adsorption stage, in order to be able to process the entire incoming flow. Each fixed bed is 2.5 m in diameter and 10 m high (Fig. 5), which present a surface-to-volume ratio of 1.6, being able to consider it an isothermal operation in the adsorption stage. The total internal volume of each fixed bed is 49 m^3, which are completely filled with Basolite C300. The bulk density of the adsorbent is 350 kg/m^3, so the total mass of adsorbent in each bed is 17.2 tons, which allow adsorbing 9.3 kg of methane by cycle in equilibrium at 0.57% CH_4 in air and 298 K.

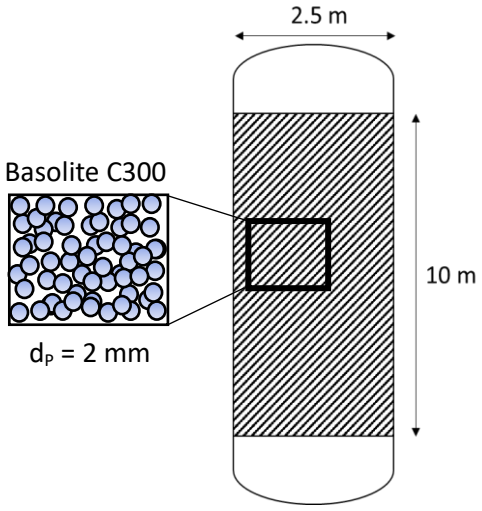

Figure 5. Outline of the fixed-bed dimensions.

3.2. Adsorption/Desorption setup

TSA cycles can be divided in four sequential steps: adsorption, heating, desorption and cooling. In case of adsorption, the inlet stream pass through the fixed bed, filled with Basolite C300, at low temperature. The material begins to adsorb methane, following kinetic and thermodynamic rules, describing a typical breakthrough curve, whose final plateau indicates the full saturation of the material. In these cases, a common technique consists of situating two or more fixed beds in series in the same stage [46]. This disposition allows to be constantly saturating one of the fixed beds, obtaining air practically pure at the outlet, since the second fixed bed is always practically fresh. On the other hand, the inlet stream to the fixed bed at desorption stage is counterflow air at high temperature. It passes through the saturated fixed bed, and the exothermic nature of the adsorption allows to desorb the compounds previously retained, also following kinetic and thermodynamic rules. The desorption fixed bed is situated in parallel to the fixed beds working in adsorption stage. Therefore, the final setup consists of 3 equal fixed beds, 2 in series in adsorption and 1 in parallel in desorption stage, working at the same time. Once the first adsorption bed is saturated, it passes to the desorption stage, and the originally second bed passes to the first position, followed by the third fixed bed that was in desorption. In order to deal with all the inlet flow, 4 identical blocks composed by these three fixed beds are situated in parallel, that is, 12 equal fixed beds working in the process. Fig. 6 depicts an scheme of two TSA process blocks with that disposition.

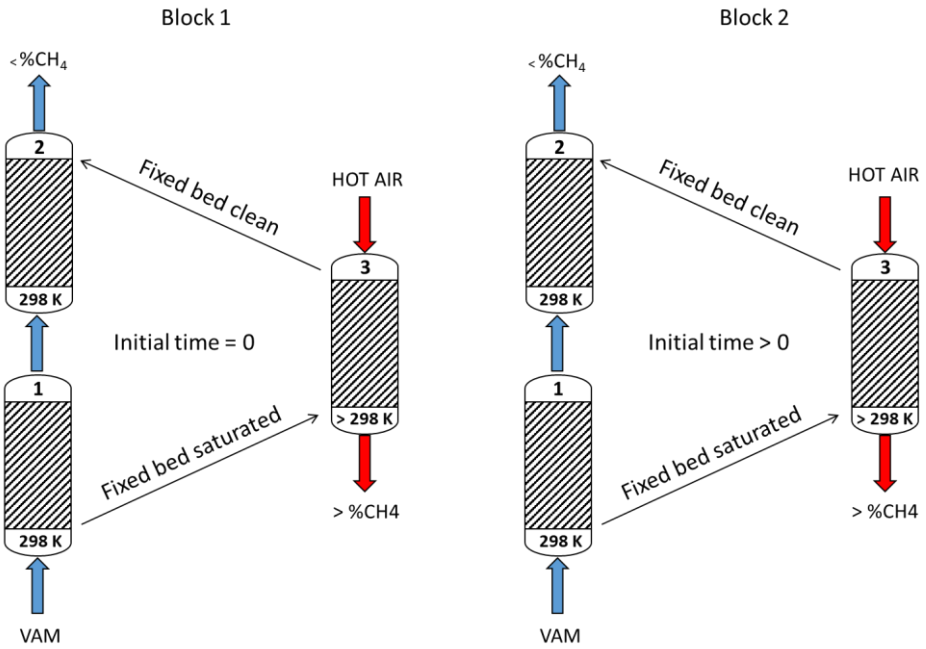

Figure 6. Scheme of two TSA process blocks. Adsorption stage with two fixed beds in series (1, 2) and desorption stage with one fixed bed in parallel (3). Initial time between blocks is different. Black arrows point out changes in fixed bed positions after clean and saturation processes are completed.

These fixed bed exchanges are made by programmed valve changes at the required times. Fig. 7 shows the set of valves and the fixed beds distribution for two fixed bed in series in adsorption stage (1 and 2) and another in parallel in desorption (3). It should be also noted that prior to the start of the adsorption, some time is required to adapt the temperature to each fixed bed (cooling) after the desorption. In case of heating, the drag stream at elevated temperature heats the solid adsorbent at the same time that desorption operation takes place.

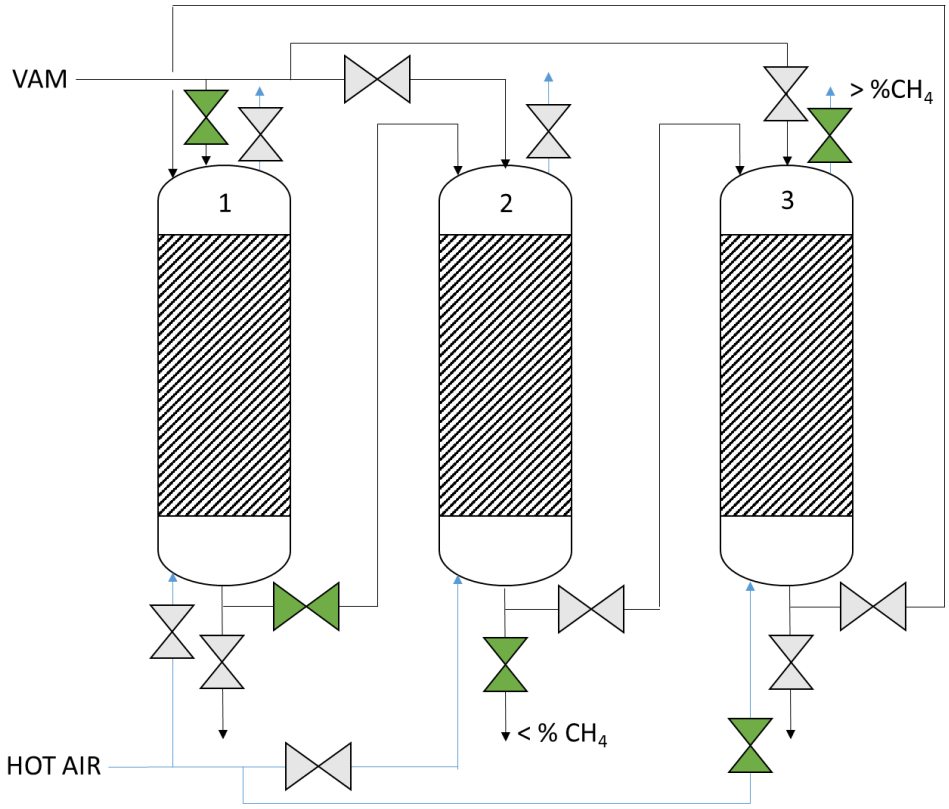

Figure 7. Schematic distribution of a TSA process with two fixed beds in adsorption (1, 2) and one fixed bed in desorption (3) stages. Black line symbolizes adsorption route, whereas blue line the desorption one. Valves in green are open, valves in grey are closed.

3.3. TSA process simulation and optimization

From the above-mentioned initial assumptions and the data included in Table 3, it is possible to obtain results for simple single-bed adsorption and desorption processes. In case of adsorption, the breakthrough curve is presented in Fig. 8A. As it is observed, necessary time for reaching the bed saturation is about 6000 s. Final methane concentration in the solid after saturation at 298 K is $3.8 \cdot 10^{-5}$ kmol/kg. Once the fixed bed in adsorption is saturated, it passes to desorption stage. Desorption curve is presented in Fig. 8B. Starting from the final concentration in the solid resulting of adsorption stage, it is possible to obtain a maximum concentration of methane at the outlet of desorption of 1.3% CH_4. The outlet has higher concentration than the inlet of the process during 1459 s, which are usable. The rest, until have cleaned completely the fixed bed (2500 s), can be discharged directly to the atmosphere due to its low methane content (~ 100% air). It is estimated that the atmospheric losses of methane through this purge are 6.9% of the total methane desorbed. The final selected desorption temperature (343 K) is reached at the half of the stage, approximately, but the average temperature during all the desorption (342 K) is close to it (Fig. 8B).

Table 3. Parameters introduced in Aspen Adsorption for the simulations

Process	Parameter	Values CH_4	Units
Adsorption	Bed length	10	m
	Bed diameter	2.5	m
	Bed porosity	0.4	-
	Bed density	350	kg/m^3
	Particle diameter	2	mm
	Mass transfer coefficients	0.012	1/s
	Molecular diffusivity	$2.2 \cdot 10^{-5}$	m^2/s
	Micropore diffusivity	$2 \cdot 10^{-10}$	m^2/s
	q_m	5.12	mol/kg
	K_L	1.16	bar^{-1}
	T	298	K
Desorption	Bed length	10	m
	Bed diameter	2.5	m
	Bed porosity	0.4	-
	Bed density	350	kg/m^3
	Particle diameter	2	mm
	Mass transfer coefficients	0.136	1/s
	Molecular diffusivity	$2.81 \cdot 10^{-5}$	m^2/s
	Micropore diffusivity	$2.26 \cdot 10^{-9}$	m^2/s
	q_m	5.12	mol/kg
	K_L*	0.244	bar^{-1}
	C_{ps}	0.755	J/g·K
	h_s	222.1	$W/m^2 \cdot K$
	a_p	6000	m^{-1}
	T	298-343	K

* Function of temperature

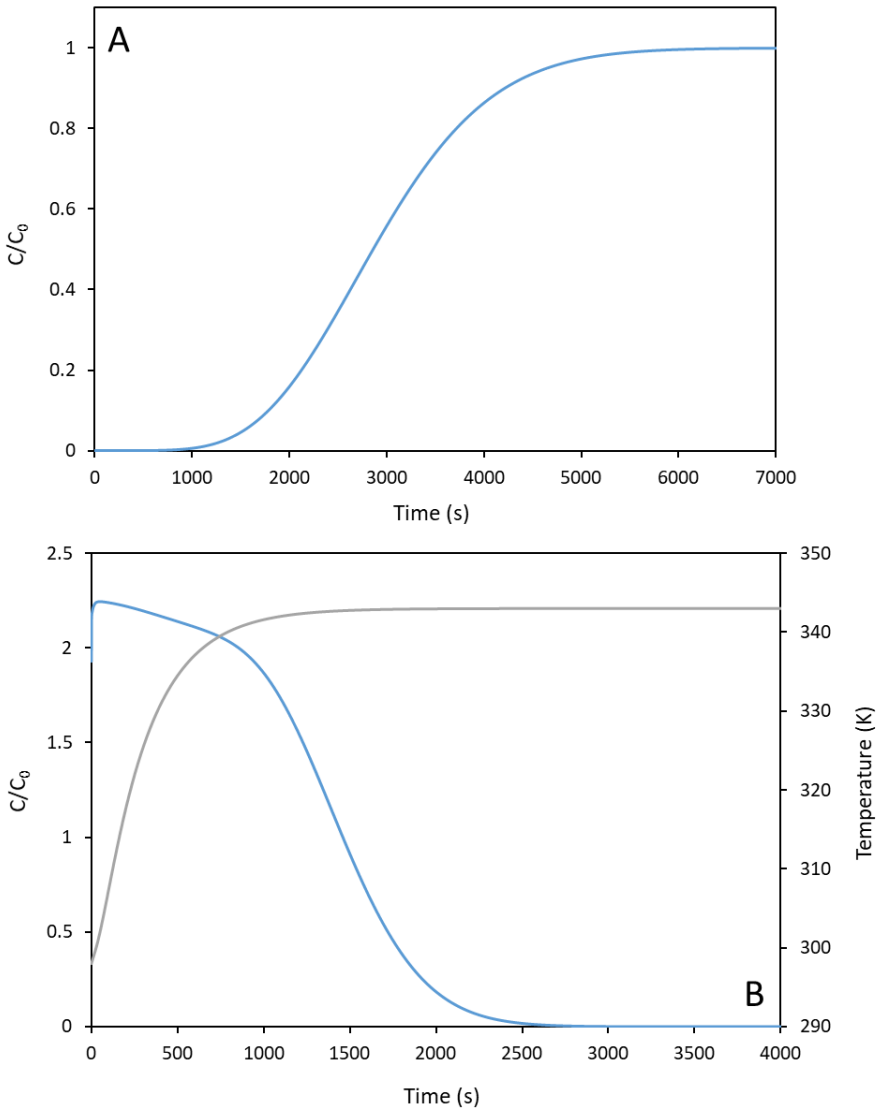

Figure 8. Methane curves of adsorption (A) and desorption (B) for a single-bed adsorption process. Solid temperature is indicated in Figure B (grey line). C_0 is the methane inlet concentration in the process.

Concerning the process optimization, the final part in a process design is the selection of the optimum value for each parameter that makes the best performance. Table 2 shows how each design parameter affects the adsorption and desorption final performances, and the typical range of each one. Adsorption and desorption are two consecutive stages, so the optimization should be first for the adsorption stage and then for the desorption one. In case of adsorption, there are five parameters that affect greatly the performance: bed length, bed diameter, surface velocity, particle diameter and temperature. In case of temperature, the adsorption is more effective the lower the operation temperature, since it is an exothermic process. Both the lower limit and the selected temperature is the ambient temperature (supposed 298 K),

because a cooling stage below that temperature would be economically unaffordable. In case of surface velocity and bed diameter, Fig. 9 shows the differences in performance for different values of both parameters.

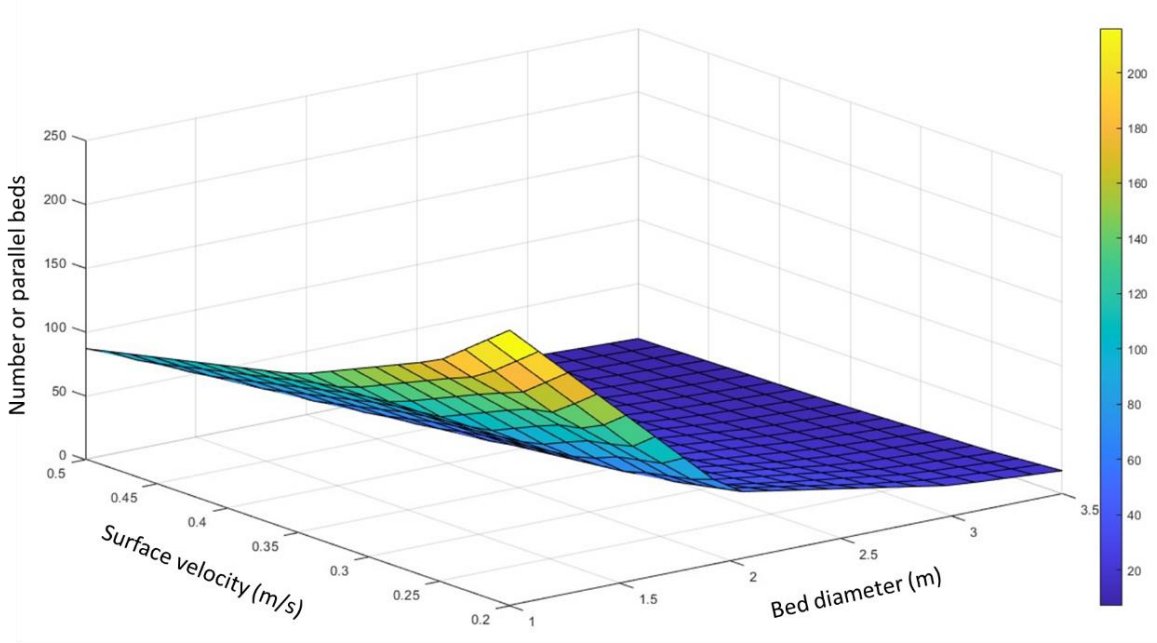

Figure 9. Relation between surface velocity, bed diameter and the number of necessary fixed beds in parallel for treating all the inlet flow (4.4 m^3/s and 0.57% CH_4) in the adsorption stage.

Surface velocity affects the breakthrough time and the pressure drop along the fixed bed, but it does not affect the final equilibrium values onto the solid. In addition, surface velocity is closely linked to the fixed bed diameter. For a constant surface velocity, the bed diameter defines the number of necessary fixed beds for covering all the inlet flow and vice versa, for a constant bed diameter, it is the surface velocity which defines the necessary parallel fixed beds. It is highly recommendable not to use a large number of fixed beds in parallel, both by total costs and also by available space. All this data allow to optimize the design of the fixed bed for adsorption stage, which consists of a group of 8 fixed beds of 2.5 m in diameter and 10 m in length, filled with Basolite C300 of 2 mm of particle diameter, with a surface velocity of 0.24 m/s and a consequent pressure drop of 0.1 bar for each one.

The next step consists on performing the parametric study for the desorption step. The fixed bed is the same, so the bed length, bed diameter and the particle size are already defined. This leaves two main parameters to consider, the surface velocity of the drag gas and the desorption temperature. The combination of both parameters affects the total amount of methane that is desorbed, as well as the duration of such desorption, i.e. its final

concentration (Fig. 10). The figure shows lower usable desorption time with higher surface velocity and lower temperature. In addition, simulations show that average methane outlet concentration is higher for large surface velocities, but the total moles of methane desorbed are lower. Final selection consist of four fixed bed parallel to adsorption ones, working at 343 K with a surface velocity of 0.48 m/s and a usable time of 1459 s for each cycle, with a maximum outlet concentration of 1.3% CH_4.

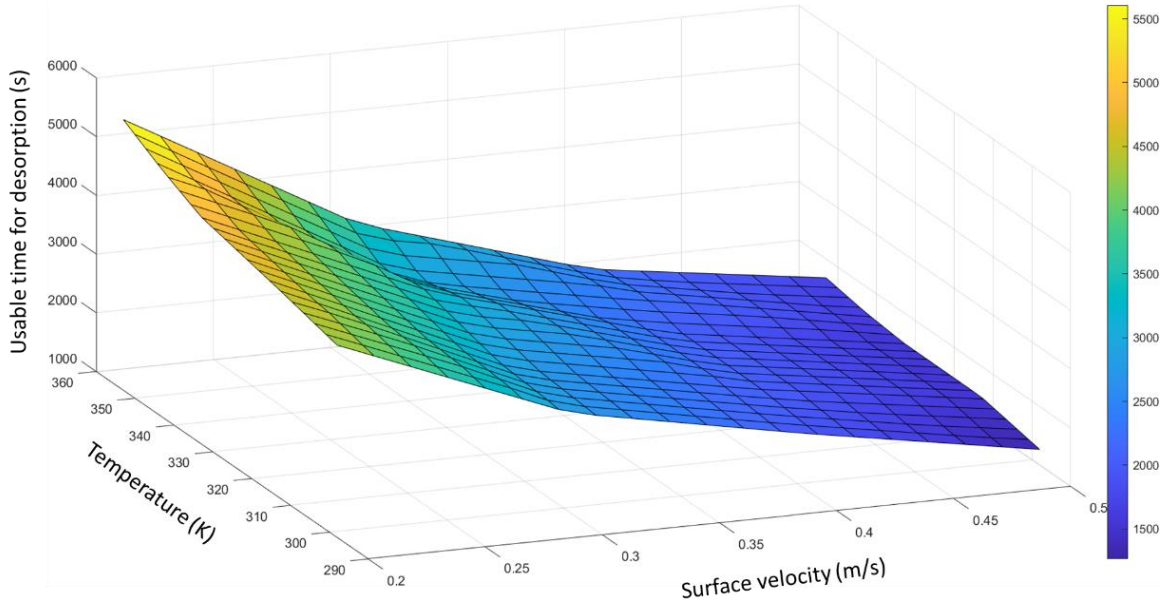

Figure 10. Relation between surface velocity, desorption temperature and the time necessary for making the usable part of desorption in the designed fixed bed (2.5 m in diameter and 10 m length).

Finally, in addition to the simple simulation of the stages (Fig. 8), it is necessary to couple all the stages in the same timeline, in order to get a continuous stream with the maximum methane content as possible. The first part is the operation of two fixed beds in series in the adsorption stage. The second fixed bed situated in series starts the adsorption (2500 s) before the complete saturation of the first fixed bed (6000 s), due to not all the methane is adsorbed by the first fixed bed with a complete efficiency. First fixed bed reaches saturation at 6000 s, but the second, instead of reaching it at 12000 s, reaches it at 8500 s (Fig. 11). Then, desorption process takes 2500 s itself, but another 1000 s are added for the cooling stage until reaching solid adsorption temperature (298 K) before starting a new cycle. On the other hand, third bed starts adsorption after saturation of the first bed (6000 s) and it is saturated at 12000 s, time when desorption begins. These three fixed beds presented in Fig. 11 make up 1 of the 4

independent blocks working in parallel, which are all equal. The time required for each stage will allow successfully coupling one bed with another, thus being able to carry out a continous process without waiting times. In addition, as seen in Fig. 8B, outlet stream from desorption stage possesses a highly variable methane concentration, between 0.57% and 1.3% CH_4, not being valid to work with the turbine a concentrations less than 1% CH_4. In order to take advantage of the maximum gas flow as possible, a common practice is to desynchronize the starting time between fixed beds in the same stage, in order to obtain a continous flow of the product, in addition to a more homogeneous final adsorbate concentration. This causes the turbine to be always fed, without waiting times. The optimum desynchronization time is 625 s between one block and the following. This disposition allow obtaining an average methane concentration at the outlet of 1.2% CH_4 and an average continous product flow of 3.8 Nm^3/s at 343 K. In addition, the introduction of an energy balance in the mathematical model allows showing also solid temperature variations during the process in the same simulation (Fig. 12).

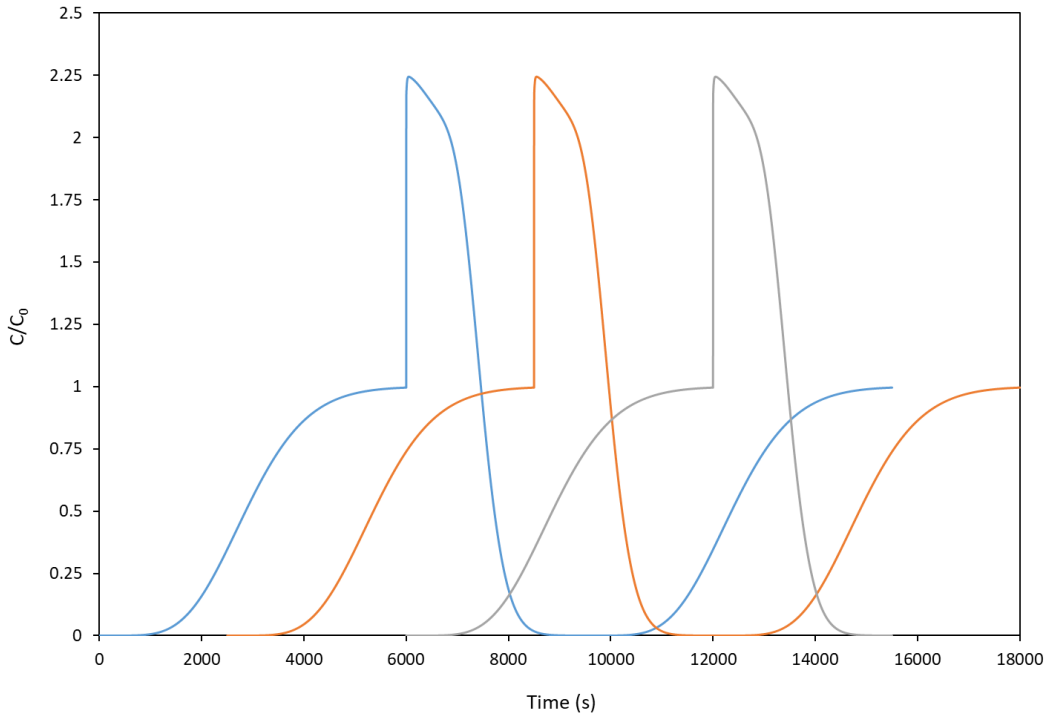

Figure 11. Simulation of a complete cycle for a TSA process with 3 fixed beds of 1 independent block. Fixed bed 1 (blue line) and fixed bed 2 (orange line) are initially in adsorption in series, whereas fixed bed 3 (grey line) is in desorption stage in parallel. C_0 is the methane inlet concentration.

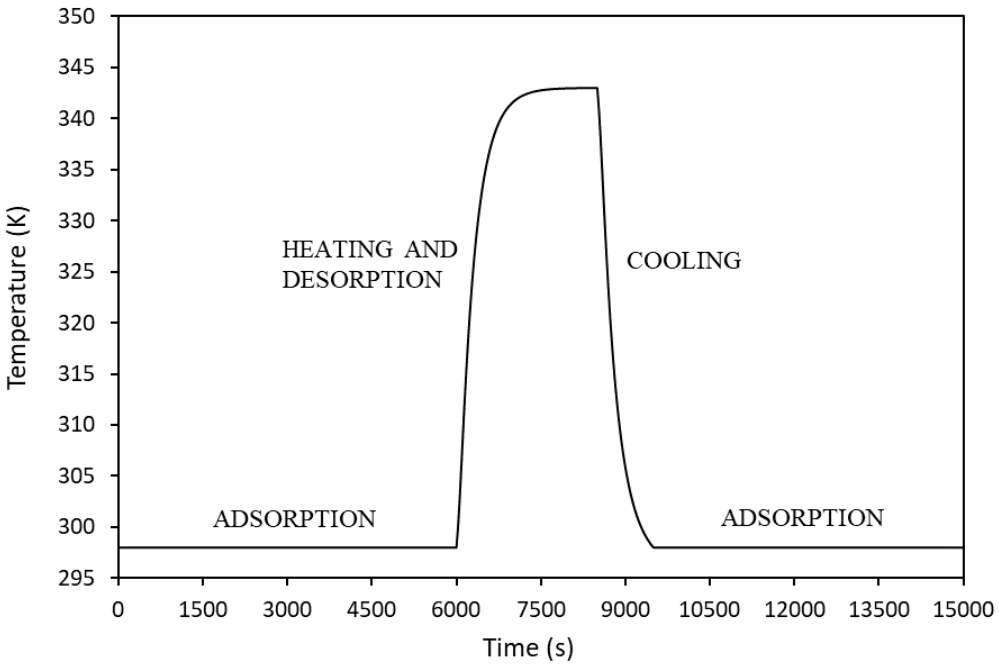

Figure 12. Adsorbent temperature variations during a TSA cycle for one of the fixed beds used.

3.4. Lean-burn turbine

As detailed in the previous section, a gas stream of 3.8 Nm^3/s containing 1.2% CH_4 at 343 K and 100 kPa is generated during the desorption step. This stream is the feed to the gas turbine and set as process specification in the following calculations. Note that methane concentration is low (1.2%), but it is above the minimum limit (1%), for which special turbines suitable for lean conditions can be used. The design of the lean-burn turbine has been carried out using Aspen Hysys for simulate the turbine behaviour. The used model was detailed in the methodology section.

In this simulation, there is just one degree of freedom for the process design: the pressure ratio of the compressor. Hence, a sensitivity analysis of this variable has been done in the range 1.1 to 3.8. On increasing the pressure ratio, the power consumed in the compressor and generated in the expander increases, but overall a higher net work (i.e., electricity) is produced in the gas turbine. However, the temperature difference between the hot and cold streams in the recuperator decreases on increasing the pressure ratio, as shown in Fig. 13. This causes an increase of the heat exchange area required in the recuperator. The minimum thermodynamic limit is a temperature difference of zero, which is achieved for a pressure ratio of 3.8 for this particular case. However, a reasonable minimum temperature difference for gas-to-gas heat transfer is 298 K, which corresponds to a pressure ratio of 3.3. This value is more realistic as the maximum recommended pressure ratio in this simulation.

The trade-offs of the pressure ratio on the annual benefit of the gas turbine can be examined in Fig. 13. The annual benefit (B) has been calculated by means of a simple economic balance:

$$B = I - E = I - C\left[\frac{i\,(1+i)^n}{(1+i)^n - 1}\right]$$

Where the annual income (I) is obtained from the electricity generated by the turbine (0.07 €/kWh) and the annual expenses (E) are mainly due to redemption of capital costs (C) (a payout time n = 15 years and discount rate i = 4.25% are used to annualize the capital costs, as shown in the equation). The main capital costs of the gas turbine are due to the compressor, expander and recuperator, as summarized in Table 4 [49]. These costs have been calculated using the results of the process simulation carried out in Aspen Hysys.

Fig. 13 shows a clear maximum on the annual benefit of the gas turbine for a pressure ratio of 2.4. For this value, the annual benefit of the gas turbine is estimated as 164 500 €/year and the temperature difference in the recuperator is 360 K, which is much higher than the minimum recommended of 298 K for gas-gas heat transfer. Note that the optimum pressure ratio of 2.4 is very close to the range recommend in the literature (2.2 to 2.3) for a similar methane concentration (0.8%) [17].

According to the results of the sensitivity analysis, the gas turbine has been designed for the optimum pressure ratio of 2.4. The power required by the compressor is 640 kW, while the power generated in the expander is 1130 kW. Consequently, the net work produced by the gas turbine is 490 kW.

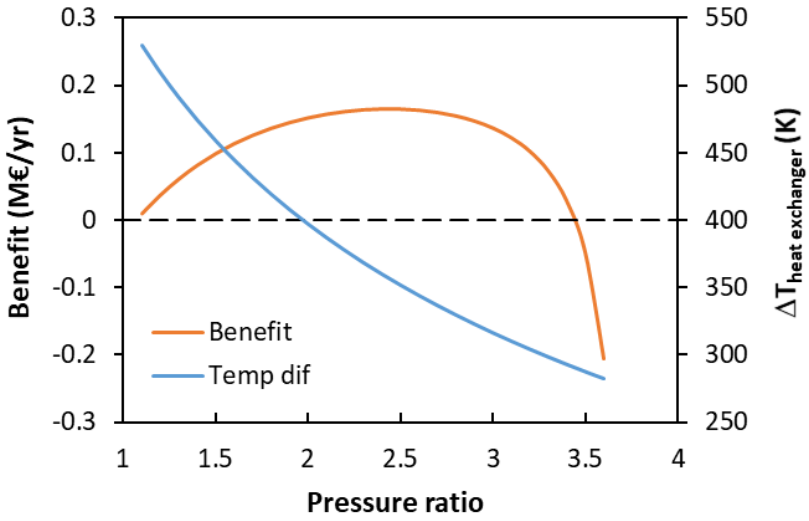

Figure 13. Sensitivity analysis of the compressor pressure ratio on the performance of the gas turbine.

4. ECONOMIC EVALUATION

In addition to yield criteria, projects must prove to be economically viable in order to be implemented or even tested on a larger scale. The entire design done throughout the work includes the material and devices needed to carry out the whole project. The economic evaluation has been done using the guidelines provided by the US Environmental Protection Agency (EPA). This organization has published a document entitled "Air Pollution Control Cost Manual" [50], which provides guidance for the design and costing of the equipment used for pollution control. This manual addresses the case of volatile organic compound abatement using adsorption and provides specific costing correlations for this equipment (they are obtained by average of vendor quotations). Apart from the equipment cost, it is also included a reference to estimate the capital investment and annual operating costs, specifically for environmental protection.

The cost of the Main Equipment are summarized in Table 4. All the costs have been updated to 2019 prices in Euro using CEPCI (Chemical Engineering Plant Cost Index). The cost of the vessel used in the adsorption unit operation is calculated using $C = 2310\ S^{0.778}$, where *C* is the cost of one unit in Euro and *S* is the external surface area (in m^2) [50]. The cost of the fan used in the adsorption step of the process is estimated as 6 577 € for the given gas flow rate of 4.41 Nm^3/s [49]. For the gas turbine, the costs are based on the power (*W* in kW) of the compressor and the expander, and the recuperator area (*A* in m^2) [49]. The total Main Equipment Cost is 2.31 M€.

Table 4. Main equipment cost of the integrated adsorption and gas turbine.

EQUIPMENT COST		
Adsorption vessel	$C_{vessel} = 2310\ N\ S^{0.778}$	820 586 €
Fan		6 577 €
Gas turbine: compressor	$C_{comp} = 1663\ W^{0.9195}$	622 588 €
Gas turbine: expander	$C_{exp} = 4454\ W^{0.5889}$	279 740 €
Recuperator	$C_{hx} = 161\ A$	583 541 €
Total equipment cost		2 313 031 €

The Main Equipment Costs exclude the piping, instrumentation and auxiliary equipment. These costs are accounted for as direct costs of the Capital Investment, which are estimated as a function of the total Cost of Main Equipment [50]. Final calculated Total Capital Investment

(TCI) is 4.74 M€. The Annual Operating Costs have also been estimated (see Table 5) [50]. These costs include labour, materials, maintenance, utilities or administrative charges. A yearly operation of the plant of 8000 h has been considered in the calculations. Additionally, it should be also considered as Annual Operating Cost the necessary replacement of the adsorbent used, since these materials have a lifetime that is lower than of the main equipment, such as, vessels or fans. It has to be replaced periodically, due to degradation and loss of capacity. For this reason, its cost must be divided and accounted for as annual following the recommendations of the EPA, considering a lifetime of n = 4 years and an interest rate of i = 4.25%, which results in a factor FWF = 0.2346. An additional 8% is added to account for freight and taxes. The cost of the adsorbent is a key parameter in the economic study, so a sensitivity analysis will be performed in order to study the viability of the process depending on it. From now, an arbitrary X value is considered for the cost of one kg of the adsorbent material.

The utilities consist of electricity consumed by the fan, which provides the head required to move the required gas flow rate through the different equipment. Considering an electricity price of 0.07 €/kWh and the power consumption of the fan (147 kW), the annual electricity consumption cost is estimated as 82 320 €/year (Table 5). However, the gas turbine is able to generate 490 kW of net work, directly as electricity. This power should be discounted from that consumed by the process. Considering the same electricity price, the gas turbine generates an earnings of 274 288 €/year, which are included as negative costs in Table 5. As shown, the total annual cost depends heavily on the adsorbent material cost (X).

In addition to the costs reflected in previous tables, it should be taken into account the positive environmental impact of the process. This is accounted for by the carbon emission allowances. Thus, the oxidation of methane to carbon dioxide in the ventilation air reduces the greenhouse gas emissions in 14 479 t CO_2-e/year (t CO_2-e means equivalent CO_2 tons). Considering a price of CO_2 of 19.71 €/t CO_2-e, the savings in emissions allowances is of 285 380 €/year. The corrected cash flow is calculated as the difference of the savings in emissions allowances (income) and the total annual cost, (52 295·X - 389 232 €/year).

Therefore, from this value of annual cash flow, it is possible to make a sensitivity analysis of the adsorbent cost per kilogram (X). As a first approximation, the value necessary for a cash flow of zero would be 7.45 €/kg. Fig. 14 shows the trends of cash flows and Net Present Value (NPV) for different adsorbent costs (X). NPV is estimated for a 20-year period based on a discount rate of 4.25%. From adsorbent costs lower than 0.6 €/kg, the process starts being profitable. In case of activated carbons, there are materials that in large quantities can reach 0.1 €/kg, but it is difficult to reach necessary selectivity and adsorption capacity specifications

despite the great variety of raw materials [51]. On the other hand, in case of MOFs, it is difficult to obtain them at such low prices, since they are synthesized almost exclusively in small batches for laboratory work. A future implementation of large-scale synthesis will make this process economically viable, which is an incentive to try to produce these materials with lower costs.

Table 5. Annual operating costs of the integrated adsorption and gas turbine.

ANNUAL OPERATING COSTS		
Direct Annual Cost	8000 h/year	
Operating Labour		
Operator	0.5 h/shift	12 925 €
Supervisor	15% operator	1 939 €
Operating Materials	-	
Maintenance		
Labour	0.5 h/shift	13 191 €
Materials	100% labour	13 191 €
Adsorbent replacement		52 295·X €
Utilities		
Electricity consumed	0.07€/kWh	82 320 €
Electricity generated	0.07€/kWh	-274 288 €
Total Direct Annual Costs		52 295·X – 150 722 €
Indirect Annual Cost		
Overhead	60% op. maint.	24 747 €
Administrative charges	2% TCI	94 873 €
Property taxes	1% TCI	47 437 €
Insurance	1% TCI	47 437 €
Capital recovery		-167 623 €
Total Indirect Annual Cost		46 870 €
Total Annual Cost		52 295·X – 103 852 €

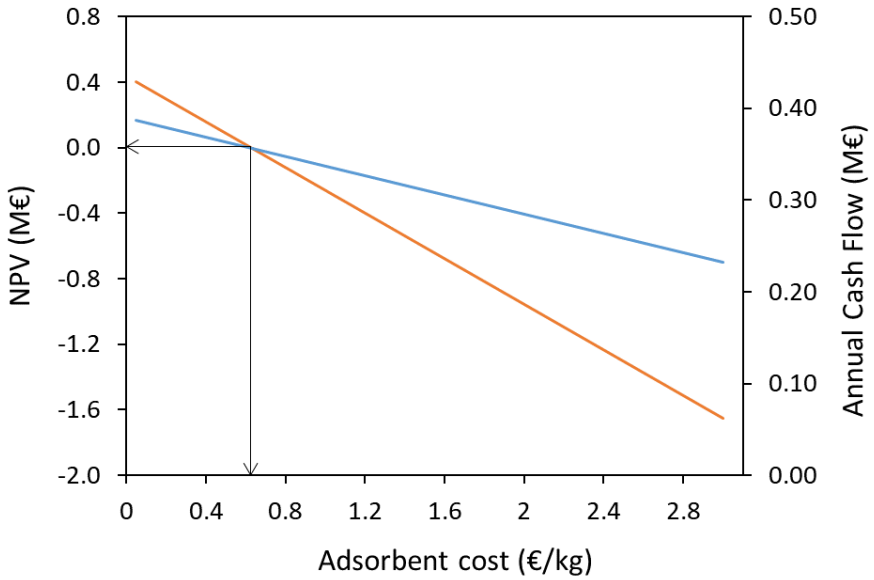

Figure 14. Results of the economic evaluation for different adsorbent costs (X). Annual cash flow (blue line), NPV (orange line). Black arrows point out the necessary adsorbent cost to make the NPV equal to zero.

5. CONCLUSIONS

This work has studied the feasibility of harnessing low-concentrated methane streams by integrating two independent processes: temperature swing adsorption for methane concentration, followed by combustion in a lean-fuel burn turbine for obtaining a surplus of electricity and calorific energy. The design has been made for a VAM inlet stream, which has a flowrate of 4.4 m^3/s, with an average methane concentration of 0.57% CH_4 in air. In relation to the adsorption/desorption unit, the simulations of Aspen Adsorption software have shown satisfactory results when working with 4 parallel blocks made up of 3 equal fixed beds each (2 in series in adsorption and 1 in parallel in desorption stage). A proper selection of the adsorbent (Basolite C300), the adequate sizing of the beds (2.5 x 10 m), as well as, the desynchronization of the bed blocks (625 s) make it possible to obtain an increase of 52.5% in methane concentration. The combustion turbine, simulated using Aspen Hysys, has also exhibited good performance, when fed with the concentrated methane stream obtained in the adsorption/desorption unit. It is selected an optimum pressure ratio of 2.4, which implies a total net-work of 490 kW. Therefore, it is obtained a satisfactory mass and energy integration between both process operations. Despite the good operational results, after in-depth economic analysis of the integration, the process shows a great dependence of the adsorbent cost. This cost should not exceed 0.6 €/kg for the process to be economically feasible (NPV = 0). This leads to the conclusion that the studied process is viable in practice, but it is

required to develop adsorbents that are at mid-point of the performance/cost relation. Thus, a larger implementation of MOFs is required on an industrial scale to lower their market price, as they are able to obtain such good results in complex separations and harnessing processes.

Acknowledgements

This work has been financed by the Research Fund for Coal and Steel of the European Union (contract RFCS2016/754077-METHENERGY+).

6. REFERENCES

[1] S. Fletcher, H. Schaefer. Rising methane: A new climate challenge. Science 364 (2019) 932-933. https://doi.org/10.1126/science.aax1828.

[2] M. Wahlen. The global methane cycle. Annual Review Of Earth And Planetary Sciences 21 (1993) 407-426. https://doi.org/10.1146/annurev.ea.21.050193.002203.

[3] D. Uprety, V. Reddy, J. Mura. Greenhouse gases: A historical perspective: A historical analysis. Climate Change and Agriculture (2019). https://doi.org/10.1007/978-981-13-2014-9_3.

[4] D. Zhong, W. Wang, Z. Zou, Y. Lu, J. Yan, K. Ding. Investigation on methane recovery from low-concentration coal mine gas by tetra-n-butyl ammonium chloride semiclathrate hydrate formation. Applied Energy 227 (2018) 686-693. https://doi.org/10.1016/j.apenergy.2017.08.069.

[5] S. Seman, I. Idris, A. Abdullah, I. Shamsudin, M. Othman. Optimizing purity and recovery of biogas methane enrichment process in a closed landfill. Renewable Energy 131 (2019) 1117-1127. https://doi.org/10.1016/j.renene.2018.08.057.

[6] J. Kim, A. Maiti, L. Lin, J. Stolaroff, B. Smit, R. Aines. New materials for methane capture from dilute and medium-concentration sources. Nature Communications 4 (2013) 1694. https://doi.org/10.1038/ncomms2697.

[7] C. Karacan, F. Ruiz, M. Cotè, S. Phipps. Coal mine methane: A review of capture and utilization practices with benefits to mining safety and to greenhouse gas reduction. International Journal of Coal Geology 86 (2011) 121-156. https://doi.org/10.1016/j.coal.2011.02.009.

[8] D. Cluff, G. Kennedy, J. Bennett, P. Foster. Capturing energy from ventilation air methane a preliminary design for a new approach. Applied Thermal Engineering 90 (2015) 1151-1163. https://doi.org/10.1016/j.applthermaleng.2015.05.013.

[9] S. Erdogan, C. Karacan, E. Okandan. Use of reservoir simulation and in-mine Ventilation measurements to estimate coal seam properties. International Journal of Rock Mechanics and Mining Sciences 63 (2014) 148-158. https://doi.org/10.1016/j.ijrmms.2013.08.008.

[10] S. Su, A. Beath, H. Guo, C. Mallett. An assessment of mine methane mitigation and utilisation technologies. Progress in Energy and Combustion Science 31 (2005) 123-170. https://doi.org/10.1016/j.pecs.2004.11.001.

[11] K. Spokas, J. Bogner, J. Chanton, M. Morcet, C. Aran, C. Graff, Y. Golvan, I. Hebe. Methane mass balance at three landfill sites: What is the efficiency of capture by gas collection systems?. Waste Management 26 (2006) 516-525. https://doi.org/10.1016/j.wasman.2005.07.021.

[12] Y. Cheng, L. Wang, X. Zhang. Environmental impact of coal mine methane emissions and responding strategies in China. International Journal of Greenhouse Gas Control 5 (2011) 157-166. https://doi.org/10.1016/j.ijggc.2010.07.007.

[13] K. Baris. Assessing ventilation air methane (VAM) mitigation and utilization opportunities: a case study at Kozlu Mine, Turkey. Energy for Sustainable Development 7 (2013) 13-23. http://dx.doi.org/10.1016/j.esd.2012.09.002.

[14] I. Karakurt, G. Aydin, K. Aydiner. Mine ventilation air methane as a sustainable energy source. Renewable and Sustainable Energy Reviews 15 (2011) 1042-1049. https://doi.org/10.1016/j.rser.2010.11.030.

[15] S. Su, J. Han, J. Wu, H. Li, R. Worrall, H. Guo, X. Sun, W. Liu. Fugitive coal mine methane emissions at five mining areas in China. Atmospheric Environment 45 (2011) 2220-2232. https://doi.org/10.1016/j.atmosenv.2011.01.048.

[16] J. Yin, S. Su, X. Yu, Y. Weng. Thermodynamic characteristics of a low concentration methane catalytic combustion gas turbine. Applied Energy 87 (2010) 2102-2108. https://doi.org/10.1016/j.apenergy.2009.12.011.

[17] S. Su, X. Yu. A 25 kWe low concentration methane catalytic combustion gas turbine prototype unit. Energy 79 (2015) 428-438. https://doi.org/10.1016/j.energy.2014.11.031.

[18] S. Ouyang, S. Xu, N. Song. Activated carbons for ventilation air methane enrichment by vacuum pressure swing adsorption. Advanced Materials Research 773 (2013) 907-911. https://doi.org/10.4028/www.scientific.net/AMR.773.907.

[19] J. Chen, J. Buege, F. Cunningham, J. Northam. Scale-up of column adsorption process by computer simulation. Industrial and Engineering Chemistry Process Design and Development 7 (1968) 26-31. https://doi.org/10.1021/i260025a006.

[20] P. Gao. The research progress of the enrichment of ventilation air methane (VAM). International Conference on Environmental Protection, Coal Industry and Metallurgical Mine Safety (2019) Francis Academic Press, UK. https://doi.org/10.25236/epcimms.2019.14.

[21] A. Ghosal, S. Manjare. Selection of appropriate adsorption technique for recovery of VOCs: an analysis. Journal of Loss Prevention in the Process Industries 15 (2002) 413-421. https://doi.org/10.1016/S0950-4230(02)00042-6.

[22] M. Clausse, J. Bonjour, F. Meunier. Adsorption of gas mixtures in TSA adsorbers under various heat removal conditions. Chemical Engineering Science 17 (2004) 3657-3670. https://doi.org/10.1016/j.ces.2004.05.027.

[23] W. Zhou. Methane storage in porous metal-organic frameworks: current records and future perspectives. The Chemical Record 10(3) (2010) 200-204. https://doi.org/10.1002/tcr.201000004.

[24] H. Wu, J. Simmons, Y. Liu, C. Brown, X. Wang, S. Ma, V. Peterson, P. Southon, C. Kepert, H. Zhou, T. Yildirim, W. Zhou. Metal-organic frameworks with exceptionally high methane uptake: where and how is methane stored?. Chemistry - A European Journal 16 (2010) 5205-5214. https://doi.org/10.1002/chem.200902719.

[25] X. Lin, N. Champness, M. Schröder. Hydrogen, methane and carbon dioxide adsorption in metal-organic framework materials. Functional Metal-Organic Frameworks: Gas Storage,

Separation and Catalysis. Topics in Current Chemistry 293 (2010) 35-76. https://doi.org/10.1007/128_2009_21.

[26] S. Kayal, A. Chakraborty. Activated carbon (type Maxsorb-III) and MIL-101(Cr) metal organic framework based composite adsorbent for higher CH_4 storage and CO_2 capture. Chemical Engineering Journal 334 (2018) 780-788. https://doi.org/10.1016/j.cej.2017.10.080.

[27] Z. Li, G. Xiao, Q. Yang, Y. Xiao, C. Zhong. Computational exploration of metal-organic frameworks for CO_2/CH_4 separation *via* temperature swing adsorption. Chemical Engineering Science 120 (2014) 59-66. https://doi.org/10.1016/j.ces.2014.08.003.

[28] A. García-Blanco, A. Vallone, S. Korili, A. Gil, K. Sapag. A comparative study of several microporous materials to store methane by adsorption. Microporous and Mesoporous Materials 224 (2016) 323-331. http://dx.doi.org/10.1016/j.micromeso.2016.01.002.

[29] I. Karakurt, G. Aydin, K. Aydiner. Mine ventilation air methane as a sustainable energy source. Renewable and Sustainable Energy Reviews 15 (2011) 1042-1049. https://doi.org/10.1016/j.rser.2010.11.030.

[30] S. Su, A. Beath, H. Guo, C. Mallet. An assessment of mine methane mitigation and utilisation technologies. Progress in Energy and Combustion Science 31 (2005) 123-170. https://doi.org/10.1016/j.pecs.2004.11.001.

[31] S. Villar-Rodil, R. Navarrete, R. Denoyel, A. Albiniak, J. Paredes, A. Martínez-Alonso, J. Tascón. Carbon molecular sieve cloths prepared by chemical vapour Deposition of methane for separation of gas mixtures. Microporous and Mesoporous Materials 77 (2005) 109-118. https://doi.org/10.1016/j.micromeso.2004.08.017

[32] T. Rufford, G. Watson, T. Saleman, P. Hofman, N. Jensen, E. May. Adsorption equilibria and kinetics of methane + nitrogen mixtures on the activated carbon Norit RB3. Industrial and Engineering Chemistry Research 52 (2013) 14270-14281. https://doi.org/10.1021/ie401831u.

[33] X. Li, L. Zhang, Z. Yang, P. Wang, Y. Yan, J. Ran. Adsorption materials for volatile organic compounds (VOCs) and the key factors for VOCs adsorption process: a review. Separation and Purification Technology 235 (2020) 116213. https://doi.org/10.1016/j.seppur.2019.116213.

[34] S. Bourrelly, P. Llewellyn, C. Serre, F. Millange, T. Loiseau, G. Férey. Different adsorption behaviors of methane and carbon dioxide in the isotypic nanoporous metal terephthalates MIL-53 and MIL-47. Journal of American Chemical Society 127 (2005) 13519-13521. https://doi.org/10.1021/ja054668v.

[35] J. Gutiérrez-Sevillano, J. Vicent-Luna, D. Dubbeldam, S. Calero. Molecular mechanisms for adsorption in Cu-BTC metal organic framework. The Journal of Physical Chemistry C 117 (2013) 11357-11366. https://doi.org/10.1021/jp401017u.

[36] Y. Peng, V. Krungleviciute, I. Eryazici, J. Hupp, O. Farha, T. Yildirim. Methane storage in metal-organic frameworks: current records, surprise findings, and challenges. Journal of the American Chemical Society 135 (2013) 11887-11894. https://doi.org/10.1021/ja4045289.

[37] D. Ursueguía, E. Díaz, S. Ordóñez. Adsorption of methane and nitrogen on Basolite MOFs: Equilibrium and kinetic studies. Microporous and Mesoporous Materials 298 (2020) 110048. https://doi.org/10.1016/j.micromeso.2020.110048.

[38] J. Mason, J. Oktawiec, M. Taylor, M. Hudson, J. Rodriguez, J. Bachman, M. Gonzalez, A. Cervellino, A. Guagliardi, C. Brown, P. Llewellyn, N. Masciocchi, J. Long. Methane storage in flexible metal-organic frameworks with intrinsic thermal management. Nature 527 (2015) 357-361. https://doi.org/10.1038/nature15732.

[39] Q. Wang, D. Shen, M. Bülow, M. Lau, S. Deng, F. Fitch, N. Lemcoff, J. Semanscin. Metallo-organic molecular sieve for gas separation and purification. Microporous and Mesoporous Materials 55 (2002) 217-230. https://doi.org/10.1016/S1387-1811(02)00405-5.

[40] X. Tang, Z. Li, N. Ripepi, A. Louk, Z. Wang, D. Song. Temperature-dependent diffusion process of methane through dry crushed coal. Journal of Natural Gas Science and Engineering 22 (2015) 609-617. https://doi.org/10.1016/j.jngse.2014.12.022.

[41] D. Ursueguía, E. Díaz, A. Vega, S. Ordóñez. Methane separation from diluted mixtures by fixed bed adsorption using MOFs: model validation and parametric studies. Separation and Purification Technologies 251 (2020) 117374. https://doi.org/10.1016/j.seppur.2020.117374

[42] D. Ko, M. Kim, I. Moon, D. Choi. Analysis of purge gas temperature in cyclic TSA process. Chemical Engineering Science 57 (2002) 179-195. https://doi.org/10.1016/S0009-2509(01)00358-X.

[43] T. Dantas, F. Luna, I. Silva, D. Azevedo, C. Grande, A. Rodrigues, R. Moreira. Carbon dioxide-nitrogen separation through adsorption on activated carbon in a fixed bed. Chemical Engineering Journal 169 (2011) 11-19. https://doi.org/10.1016/j.cej.2010.08.026.

[44] F. Kloutse, R. Zacharia, D. Cossement, R. Chahine. Specific heat capacities of MOF-5, Cu-BTC, Fe-BTC, MOF-177 and MIL-53 (Al) over wide temperature ranges: Measurements and application of empirical group contribution method. Microporous and Mesoporous Materials 217 (2015) 1-5. https://doi.org/10.1016/j.micromeso.2015.05.047.

[45] A. Gabelman, 2017. Adsorption basics: Part 1. https://www.aiche.org/resources/publications/cep/2017/july/adsorption-basics-part-1 (accessed 15 May 2020).

[46] J. R. Couper, W. R. Penney, J. R. Fair, S. M. Walas, 2005. Chemical process equipment: selection and design, third ed. Elsevier, Waltham (MA).

[47] J. Theuerkauf, P. Witt, D. Schwesig. Analysis of particle porosity distribution in fixed beds using the discrete element method. Powder Technology 165 (2006) 92-99. https://doi.org/10.1016/j.powtec.2006.03.022.

[48] C. Perego, S. Peratello. Experimental methods in catalytic kinetics. Catalysis Today 52 (1999) 133-145. https://doi.org/10.1016/S0920-5861(99)00071-1.

[49] Equipment Costs: Plant design and economics for chemical engineers, 2003. https://www.mhhe.com/engcs/chemical/peters/data/ (accessed 15 May 2020).

[50] Cost reports and guidance for air pollution regulations, 2018. https://www.epa.gov/economic-and-cost-analysis-air-pollution-regulations/cost-reports-and-guidance-air-pollution (accessed 15 May 2020).

[51] M. Rafatullah, O. Sulaiman, R. Hashim, A. Ahmad. Adsorption of methylene blue on low-cost adsorbents: A review. Journal of Hazardous Materials 177 (2010) 70-80. https://doi.org/10.1016/j.jhazmat.2009.12.047.

LIST OF SYMBOLS AND ABBREVIATIONS

GWP	Global warming potential
CMM	Coal mine methane
AMM	Abandoned mine methane
VAM	Ventilation air methane
TSA	Temperature swing adsorption
PSA	Pressure swing adsorption
VSA	Vacuum swing adsorption
MOFs	Metal-organic frameworks
LDF	Linear driving force
EPA	Environmental Protection Agency
CEPCI	Chemical Engineering Plant Costs Index
FWF	Future worth factor
TCI	Total capital investment
NPV	Net present value (M€)
C_i	Concentration in gas phase (mol/m^3)
t	Time (s)
u_0	Surface velocity (m/s)
ε_b	Bed porosity (-)
Z	Fixed bed axial position (m)
D_e	Axial dispersion (m^2/s)
ρ_b	Bed density (kg/m^3)
d_p	Particle diameter (m)
D_i	Micropore diffusivity (m^2/s)
W_{ieq}	Solid-gas equilibrium concentration (mol/kg)
W_i	Adsorbate concentration in solid phase (mol/kg)
T_s	Solid temperature (K)
T_g	Gas temperature (K)
h_s	Heat transfer coefficient (W/m^2·K)
C_{ps}	Solid specific heat capacity (J/kg·K)
C_{pg}	Gas specific heat capacity (J/kg·K)
ρ_g	Gas density (kg/m^3)
a_p	Adsorbent surface-to-volume ratio (m^{-1})

P_P	Adsorbate gas partial pressure (bar)
q_m	Maximum capacity (Langmuir model) (mg/g)
K_L	Langmuir isotherm constant (bar^{-1})
q_e	Equilibrium capacity (Langmuir model) (mg/g)
$K_{L(0)}$	Arrhenius equation pre-exponential term (bar^{-1})
-ΔH	Activation energy (J/mol)
R	Ideal gases constant (J/mol·K)
T	Adsorption temperature (K)
μ_g	Gas viscosity (Pa·s)
dP/dZ	Pressure drop by bed length (bar/m)
C_0	Initial concentration of the adsorbate (mol/m^3)
B	Annual benefit (€)
I	Annual income (€)
E	Annual expenses (€)
C	Capital costs (€)
n	Payout time (year)
i	Discount rate (%)
S	External surface area of the vessel (m^2)
N	Number of vessels
W	Power of gas turbine (compressor/expander) (kW)
A	Recuperator area (m^2)
C_{vessel}	Adsorption vessel cost (€)
C_{comp}	Compressor cost (€)
C_{exp}	Expander cost (€)
C_{hx}	Heat exchanger cost (€)
X	Adsorbent cost (€/kg)